

Jahn-Teller mechanism of stripe formation in doped layered $\text{La}_{2-x}\text{Sr}_x\text{NiO}_4$ nickelates

Krzysztof Rościszewski¹ and Andrzej M. Oleś^{1,2}

¹ Marian Smoluchowski Institute of Physics, Jagellonian University,
Reymonta 4, PL-30059 Kraków, Poland

² Max-Planck-Institut für Festkörperforschung,
Heisenbergstrasse 1, D-70569 Stuttgart, Germany

E-mail: krzysztof.rosciszewski@uj.edu.pl; a.m.oles@fkf.mpg.de

Abstract. We introduce an effective model for e_g electrons to describe quasi-two-dimensional layered $\text{La}_{2-x}\text{Sr}_x\text{NiO}_4$ nickelates and study it using correlated wave functions on 8×8 and 6×6 clusters. The effective Hamiltonian includes the kinetic energy, on-site Coulomb interactions for e_g electrons (intraorbital U and Hund's exchange J_H) and the coupling between e_g electrons and Jahn-Teller distortions (static modes). The experimental ground state phases with inhomogeneous charge, spin and orbital order at the dopings $x = 1/3$ and $x = 1/2$ are reproduced very well by the model. Although the Jahn-Teller distortions are weak, we show that they play a crucial role and stabilize the observed cooperative charge, magnetic and orbital order in form of a diagonal stripe phase at $x = 1/3$ doping and a checkerboard phase at $x = 1/2$ doping.

Published in J. Phys.: Condens. Matter **23**, 265601 (2011).

PACS numbers: 75.25.Dk, 75.47.Lx, 75.10.Lp, 63.20.Pw

1. Introduction

The nature and origin of stripe phases in transition metal oxides continues to attract considerable attention in the theory of strongly correlated electrons. The phenomenon of stripes occurs in doped materials and, as one of few developments in the physics of superconducting cuprates, was discovered first in theory [1] before their existence was confirmed by experimental observations [2]. In a system with dominant electron-electron interactions novel phases with charge order in form of a Wigner crystal, or stripe phases with nonuniform charge distribution are expected. In the well known example of the cuprates charge order coexists with the modulation of antiferromagnetic (AF) order between alternating domains [3,4]. The stripe phases in the realistic models for cuprates were obtained, *inter alia*, by calculations using Hartree-Fock (HF) approximation [1], correlated wave functions [5], dynamical mean-field theory [6] and slave bosons [7]. These studies have shown that correlation effects play an important role in the physical properties of stripes.

The physical origin of stripes becomes more complex in systems with active orbital degrees of freedom, as in the doped manganites with e_g orbital degrees of freedom [8–10], and it was soon recognized that the mechanism of stripes has to involve charge and magnetic order coexisting with certain type of orbital order [11,12]. The mechanism of stripe formation in such systems is subtle and involves directional hopping between the orbital wave functions, in particular for t_{2g} orbital states [13], that could play a role in the properties of doped iron pnictides [14].

In contrast to the stripes in cuprates [3], the stripes in nickelates are along diagonal direction in the square lattice [15]. This by itself is puzzling and suggests that other degrees of freedom may contribute. The properties of doped perovskite nickelates are still not completely understood in spite of considerable effort put forward both in theory [12,16–21] and in experiment [22,23]. The main difficulty in the theoretical description of this class of compounds is related to simultaneous importance of numerous degrees of freedom. Unfortunately, all of them contribute and one can not argue that only some types of the interactions are essential and could be considered in a simplified approach, while the others are of secondary importance and would be responsible for quantitative corrections only. We argue that attempts to consider only some interactions, for instance either including only strong on-site Coulomb and Hund's exchange interactions and neglecting the coupling to the lattice via the Jahn-Teller (JT) distortions, or studying the coupling to the lattice distortions in absence of strong local Coulomb interactions, are both not sufficient to account for the experimental situation. The phase situation in this class of compounds is a result of a subtle balance between numerous factors.

On the theoretical side, the multiband models and/or approaches based on the *ab initio* local density approximation (LDA) computations extended by static corrections due to local Coulomb interaction U (within the LDA+ U scheme) [19,21], seem to be the most realistic and complete approaches to theoretical description of the nickel oxides with a perovskite structure. The drawback of such approaches, however, is considerable

technical difficulty to work with doped systems especially for arbitrary doping levels x because in such a case very big unit cells (or clusters) need to be considered.

Therefore it is quite helpful (and complementary to LDA+ U approaches) to identify first all physical mechanisms which are essential in doped nickelates and then develop a simplified but still well motivated effective model to describe them. In the present paper we use such an effective model (featuring only Ni sites renormalized by the presence of surrounding oxygens) for the description of itinerant e_g electrons which includes all essential interactions present in layered nickelates. We do not develop new concepts here but use the model well tested before in the manganite perovskites, including also monolayer and bilayer systems [24]. Further justification of this model follows from similar microscopic approaches developed earlier to describe doped nickelates [11, 12, 16, 18]. With this microscopic model we investigate the nature and type of coexisting magnetic, orbital and charge order in the ground state when local electron correlations and the coupling to JT distortions are both included. In this paper we focus on quasi two-dimensional (2D) monolayer nickelates $\text{La}_{2-x}\text{Sr}_x\text{NiO}_4$.

The paper is organized as follows. First, we introduce in section 2 a *realistic* model for e_g electrons in nickelate which includes the electron interactions and the local potentials due to static JT distortions. In this section we also introduce the method to treat electron correlation effects beyond the HF approximation, and discuss realistic values of model parameters. The results obtained for various doping levels are presented and analysed in section 3. Next we concentrate on the role played by the JT distortions (in section 4) and show that they are crucial for the stability of the stripe phase at the $x = 1/3$ doping. Finally we present a short summary in section 5 as well as some general conclusions.

2. The microscopic model and methods

2.1. The effective model Hamiltonian

We investigate strongly correlated electrons in doped monolayer nickelates $\text{La}_{2-x}\text{Sr}_{1+2x}\text{NiO}_4$ (with doping $0 < x < 0.5$), using an effective model describing only Ni sites, where the state of surrounding oxygens is included by an effective potential at each site. (A realistic effective Hamiltonian which acts in the subspace of low energy e_g states and the precise values of the Hamiltonian parameters can be derived by a procedure of mapping the results of HF, or LDA+ U , or all-electron *ab initio* calculations obtained within a more complete approach). A local basis at each nickel site is given by two Wannier orbitals of e_g symmetry, i.e., $x^2 - y^2$ and $3z^2 - r^2$ orbitals.

In the present study we use a Hubbard-type Hamiltonian \mathcal{H} for two e_g orbital states defined on a finite cluster:

$$\mathcal{H} = H_{\text{kin}} + H_{\text{cr}} + H_{\text{int}} + H_{\text{spin}} + H_{\text{JT}}, \quad (1)$$

which consists of kinetic (H_{kin}), crystal field (H_{cr}), on-site Coulomb (H_{int}), spin (H_{spin}), and JT (H_{JT}) terms. The variants of this microscopic model were used to describe doped

Jahn-Teller mechanism of stripe formation in doped layered $La_{2-x}Sr_xNiO_4$ nickelates 4
monolayer, bilayer and perovskite manganites [24], where the same e_g orbital degrees of freedom are present.

The kinetic part H_{kin} is expressed using two e_g orbitals:

$$|z\rangle \equiv |(3z^2 - r^2)/\sqrt{6}\rangle, \quad |x\rangle \equiv |(x^2 - y^2)/\sqrt{2}\rangle. \quad (2)$$

per site, with anisotropic phase dependent hopping which depends on the orbital phases on neighbouring sites,

$$H_{\text{kin}} = -\frac{1}{4}t_0 \sum_{\{ij\}||ab,\sigma} \left\{ (3d_{ix\sigma}^\dagger d_{jx\sigma} + d_{iz\sigma}^\dagger d_{jz\sigma}) \pm \sqrt{3}(d_{ix\sigma}^\dagger d_{jz\sigma} + d_{iz\sigma}^\dagger d_{jx\sigma}) \right\}. \quad (3)$$

Here $d_{i\mu\sigma}^\dagger$ are creation operators for an electron in orbital $\mu = x, z$ with spin $\sigma = \uparrow, \downarrow$ at site i . The $\{i, j\}$ runs over pairs of nearest neighbours (bonds); \pm is interpreted as plus sign for $\langle ij \rangle$ being parallel to the crystal axis a and minus for $\langle ij \rangle$ being parallel with to the axis b .

The kinetic energy is supplemented by the crystal field term which describes orbital splitting

$$H_{\text{cr}} = \frac{1}{2}E_z \sum_{i\sigma} (n_{iz\sigma} - n_{ix\sigma}). \quad (4)$$

For the present convention and for negative values of crystal field parameter ($E_z < 0$) the z orbital is being favored over the x orbital.

The H_{int} and H_{spin} stand for an approximate form of local Coulomb and exchange interactions for electrons within degenerate e_g orbitals used before for monolayer, bilayer and cubic perovskite manganites [24],

$$H_{\text{int}} = U \sum_{i\mu} n_{i\mu\uparrow} n_{i\mu\downarrow} + (U_0 - \frac{5}{2}J_H) \sum_i n_{ix} n_{iz}, \quad (5)$$

$$H_{\text{spin}} = -\frac{1}{2}J_H \sum_i (n_{ix\uparrow} - n_{ix\downarrow})(n_{iz\uparrow} - n_{iz\downarrow}). \quad (6)$$

On-site Coulomb interaction is denoted as U , the Hund's exchange interaction constant is J_H . Here the spin symmetry is explicitly broken, the quantization axis is fixed in spin space and the full Hund's exchange interactions with SU(2) symmetry are replaced by the Ising term. However, the above form suffices as it gives the same Hamiltonian in the HF approximation as an exact expression for two e_g orbitals [25].

The simplified JT part H_{JT} is:

$$H_{\text{JT}} = g_{\text{JT}} \sum_i \left\{ Q_{1i}(2 - n_{ix} - n_{iz}) + Q_{2i}\tau_i^x + Q_{3i}\tau_i^z \right\} + \frac{1}{2}K \sum_i \left\{ 2Q_{1i}^2 + Q_{2i}^2 + Q_{3i}^2 \right\}, \quad (7)$$

where the pseudo-spin operators, i.e., $\{\tau_i^x, \tau_i^z\}$ operators, are defined as follows

$$\tau_i^x = \sum_{\sigma} (d_{ix\sigma}^\dagger d_{iz\sigma} + d_{iz\sigma}^\dagger d_{ix\sigma}), \quad \tau_i^z = \sum_{\sigma} (d_{ix\sigma}^\dagger d_{ix\sigma} - d_{iz\sigma}^\dagger d_{iz\sigma}). \quad (8)$$

The Hamiltonian eq. (7) includes three different static JT modes, where $\{Q_{1i}, Q_{2i}, Q_{3i}\}$ denote the JT static deformation modes of the i -th octahedron. (For simplicity the harmonic constant of isotropic JT (breathing) mode Q_1 is assumed to be double with respect to those corresponding to Q_2 and Q_3 unsymmetric modes as discussed in refs. [8, 12]). Note that H_{JT} taking the above form is a simplification: (i) first, some anharmonic terms were omitted (compare for example the corresponding terms in Ref. [26]), and (ii) second, all JT distortions are treated here as independent from each other. On the contrary, in reality two neighbouring Ni atoms share one oxygen in between them, and thus neighbouring JT distortions are not really independent. The present approximation is the simplest one to describe the coupling to the local JT modes in a model where oxygen ions are not explicitly included (for a more detailed discussion see ref. [12]).

2.2. Calculations within the Hartree-Fock approximation

We performed extensive calculations for clusters with periodic boundary conditions. A systematic study of increasing doping from $x = 0$, through $x = 1/8, 2/8, 3/8$, up to $x = 4/8$ was performed for 8×8 clusters, and was supplemented by doping $x = 1/3$ for 6×6 cluster. We investigate the ground state at zero temperature ($T = 0$).

First, the calculations within the single-determinant HF approximation were performed to determine the ground state wave function. Also the gap between the highest occupied molecular orbital (HOMO) and the lowest unoccupied molecular orbital (LUMO), the HOMO-LUMO gap

$$\Delta \equiv E_{\text{LUMO}} - E_{\text{HOMO}}, \quad (9)$$

was extracted at this step. In the next step the HF wave function was modified to include the electron correlations by employing local ansatz [27], see below.

Coming to details: in the first step HF computations were run starting from one of several different initial conditions (on average a few thousands for each set of Hamiltonian parameters are necessary as the identification of a true energy minimum is difficult), i.e., from predefined (some symmetry fixed, but mostly random) charge, spin and orbital configurations and several predefined sets of classical variables $\{Q_{1i}, Q_{2i}, Q_{3i}\}$. For each fixed set of starting parameters and starting initial conditions we obtain on convergence a new HF wave function $|\Psi_{\text{HF}}\rangle$ which is a candidate for a ground state wave function. This self-consistent procedure is assumed to provide energy minimum also with respect to the classical $\{Q_{1i}, Q_{2i}, Q_{3i}\}$ variables [24].

2.3. Electron correlations

After completing the HF computations for a given wave function $|\Psi\rangle$, we performed correlation computations (second step) which provide the total energy. (For details see refs. [5, 24]). Namely the HF wave function $|\Phi_0\rangle$ was modified to include the electron

Jahn-Teller mechanism of stripe formation in doped layered $La_{2-x}Sr_xNiO_4$ nickelates 6
correlation effects. We used exponential local ansatz for the correlated ground state [27],

$$|\Psi\rangle = \exp\left(-\sum_m \eta_m O_m\right)|\Phi_0\rangle, \quad (10)$$

where $\{O_m\}$ are local correlation operators. The variational parameters η_m (four singlet and two triplet ones) are found by minimizing the total energy,

$$E_{\text{tot}} = \frac{\langle\Psi|H|\Psi\rangle}{\langle\Psi|\Psi\rangle}. \quad (11)$$

Here for the correlation operators we use

$$O_m = \sum_i \delta n_{i\mu\sigma} \delta n_{i\nu\sigma'}, \quad (12)$$

The sum in the above equation ensures smaller number of the variational parameters; on the other hand the nonhomogeneous correlations are treated in an averaged way (this procedure is somewhat similar to calculations performed within mean-field approaches). The symbol δ in $\delta n_{i\mu\sigma}$ indicates that *only that part* of $n_{i\mu\sigma}$ operator is included which annihilates one electron in an occupied single particle state which belongs to the HF ground state $|\Phi_0\rangle$, and creates an electron in one of the virtual states. The above local operators O_m correspond to the subselection of most important two electron excitations within the *ab initio* configuration-interaction method. We note that three, four, *etcetera*, electron excitations (which are omitted here) are also important in the strongly correlation regime. However, as yet there is no an easy way to implement them for a larger systems, thus one is able to implement within theory only the leading part of the correlation energy (which follows from two-particle excitations).

After obtaining the total energy for a given configuration, we repeat all the procedure from the beginning, i.e., we take the second set of HF initial conditions and repeat all computations to obtain the second candidate for a ground state wave function. Other configurations for the third, fourth, *etcetera*, set of initial conditions are investigated in a similar way. Finally, the resulting set of total energies was inspected and the lowest one was identified as the best candidate for the true ground state. In general, the correlations are found to be strong, in fact much stronger than those found in the perovskite manganites [24].

2.4. Parameters of the model

The values of the Hamiltonian parameters used below follow closely the sets commonly employed in the literature to study doped nickelates. For the effective $d-d$ hopping ($dd\sigma$) we assume $t_0 = 0.6$ eV, following ref. [18]. Local Coulomb interactions are strong, and we assume $8 < U/t_0 < 12$ (the lowering of the very large atomic value on nickel is due to an appropriate screening of the e_g electrons). Hund's exchange coupling was $J_H = 0.9$ eV [18, 19]. The crystal field values we considered were either $E_z = 0$ or $E_z = -0.3$ eV, with the latter value inducing a higher electron density in z orbitals, as expected for a single NiO_2 plane (compare with refs. [12, 18]).

Table 1. Parameters of the microscopic model eq. (1) used in most of the performed calculations (all electronic parameters $\{t_0, U, J_H, E_z\}$ in eV).

t_0	U	J_H	E_z	g_{JT} (eV \AA^{-1})	K (eV \AA^{-2})
0.6	7.0	0.9	-0.3	3.0	13.0

Very little is known about JT interactions in nickelates, therefore the JT constant K was fixed as $K = 13 \text{ eV } \text{\AA}^{-2}$ (like in manganite perovskites [24]), and the coupling constant with the lattice distortions g_{JT} was assumed to be in the range $2 \text{ eV } \text{\AA}^{-1} < g_{\text{JT}} < 3.8 \text{ eV } \text{\AA}^{-1}$, following ref. [8].

The best set of the Hamiltonian parameters which allows one to reproduce the experimental phase situation is given in table 1. In some cases, other parameter values were used as discussed below. However, the parameters one should use are constrained by the experimental observations. It is fortunate that the obtained types of spin, orbital and charge order turn out to be rather sensitive on the parameter values. In fact, many sets of the Hamiltonian parameters (different than those in table 1) were also considered in test computations but they do not generate reasonable results (i.e., the ground states with the ordering close to that reported in experiments). Although full phase diagram would be very appropriate here, it is unfortunately too expensive to compute by the present method.

3. Results

The computations were repeated for many sets of the Hamiltonian parameters and for many (up to several thousands) charge, spin, orbital and JT distortions (i.e., for local configurations required to start HF iterations). Extensive calculations were required to establish the parameter values which are realistic for doped nickelates and allow one for reproduction of basic experimental observations. Below we present the results obtained for the realistic parameter set as given in table 1.

3.1. Low doping regime

The results obtained in low doping regime are presented in figures 1-2. First we considered $x = 1/8$ doping. In $\text{La}_{2-x}\text{Sr}_{1+2x}\text{CuO}_4$ cuprates one finds at this doping level stable stripe phases [3, 5–7]. In the present case we observed isolated Ni ions with holes doped in x orbitals, as shown in figure 1. At these ions the magnetic moments are due to $S = 1/2$ spins and are therefore lower than magnetic moments at $S = 1$ sites, thus appearing as spin defects in the G -AF phase. While both x and z orbitals are occupied at undoped sites, one finds that only z orbitals are occupied at doped sites. Of course, certain delocalization of electrons between the two sublattices takes place as well in a doped antiferromagnet investigated here, but the above ionic picture applies to

a good approximation. In fact, the obtained phase is insulating with a HOMO-LUMO gap of 1.86 eV.

Local charge defects consist of z electrons occupying doped Ni^{3+} sites which couple to lattice distortions $\{Q_{i3}\}$, as shown in the lower panel of figure 1. These distortions act as self-trapping on the doped charges and suppress the kinetic energy of doped holes. Therefore, this regime of doping is manifestly different from the observations in cuprates, where JT distortions were inactive and self-organization of doped holes in form of horizontal stripes takes place [1–3].

At a higher doping $x = 1/4$ the magnetic order changes to the C -AF phase shown in figure 2, with relatively large magnetic cells. This phase is weakly insulating, with the HOMO-LUMO gap $\Delta = 0.28$ eV. Horizontal ferromagnetic (FM) lines are characterized by charge modulations between almost undoped Ni^{2+} ions and doped Ni^{2+} ions. The latter doped sites are distributed far from one another both within FM chains and between consecutive AF horizontal lines. This may be seen as a physical reason which prevents the occurrence of stripes at this doping level. Furthermore, the doped sites couple actively to local distortions, and can be identified by looking at the pattern of JT distortions, see the lower panel in figure 2. It helps to identify imperfect long-range order of doped holes which avoid each other, similar to the $x = 1/8$ doping considered above.

3.2. Diagonal stripes at doping $x = 1/3$

The case of $x = 1/3$ doping was investigated with 6×6 cluster, see figure 3. Here the number of doped sites is the same as the doping, i.e., $x = 1/3$, meaning that some of doped sites have to be located at next-nearest neighbour positions. The resulting stripe phase with diagonal lines of reduced charges (doped sites) may be therefore seen as a modification of the C -AF phase obtained at the $x = 1/4$ doping by adding more doped holes (Ni^{3+} ions). Indeed, one finds that every third site in an AF row (FM column) contains the reduced charge close to one added hole, and these sites form a (11) stripe phase. Note that the horizontal and vertical lines are here interchanged as compared with figure 2, but this configuration is of course equivalent to the one with FM horizontal lines, and AF order between them. The large JT distortions accompany the sites with minority charges, so the stripe pattern can be also recognized by analyzing them. It reproduces the experimental results in refs. [22,23], with the long-range order coexisting charge, spin and orbital order in form of diagonal stripes, present at the doping $x = 1/3$. Also this phase is insulating, with a HOMO-LUMO gap $\Delta = 0.57$ eV.

We emphasize that the JT distortions play a crucial role in the observed stripe phase at $x = 1/3$ doping. We have verified that when one switches off the JT coupling, i.e., when one puts $g_{JT} = 0$ with other parameters unchanged, the stripes vanish and the ground state becomes conducting (HOMO-LUMO gap $\Delta = 0.03$ eV), see below. In this case one finds the same magnetic phase with horizontally arranged FM lines coupled in the vertical direction in the C -AF order, with slightly nonuniform charge distribution

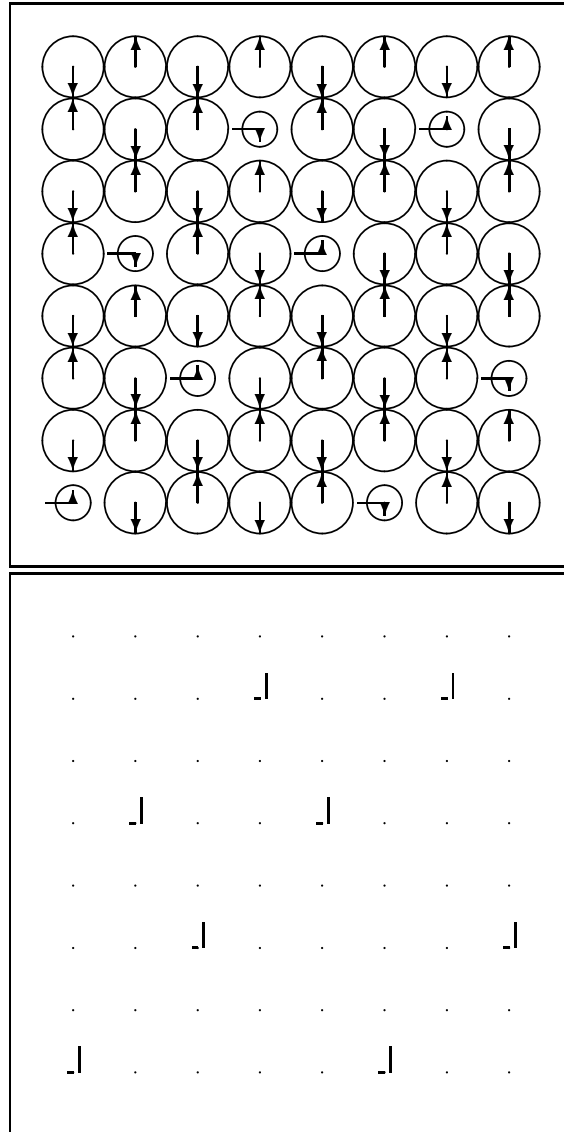


Figure 1. Insulating G -AF ($S=1$) spin arrangement, with mostly uniform charge distribution and equal electron densities within x and z e_g orbitals (no orbital order) at undoped sites as obtained for $x = 1/8$ doping in 8×8 cluster. Note 8 doped holes (charge minority sites with smaller spins) placed randomly and with z orbitals occupied by electrons. **Upper panel:** At each site the circle diameter corresponds to one-half of e_g on-site total charge; the arrow length to one-half of the e_g spin; the horizontal bar length to charge density difference between x and z orbitals (longest bar to the right corresponds to pure x , to the left to pure z , zero length to half by half combination). All these values are expressed in approximate proportionality (as generated by latex graphic package) to nearest neighbour site-site distance which is assumed to be unity. **Lower panel:** JT distortions Q_{2i} (in Å) for the same plane shown as bars drawn slightly to the left of each site and Q_{3i} , shown by bars to the right of each site. Isotropic (breathing) mode Q_{1i} in between. Q_{2i} and Q_{3i} bars are artificially enlarged (by a factor of 2) for a better visibility. The static JT distortions (finite Q_3 mode, the other modes vanish) are only present at charge minority sites.

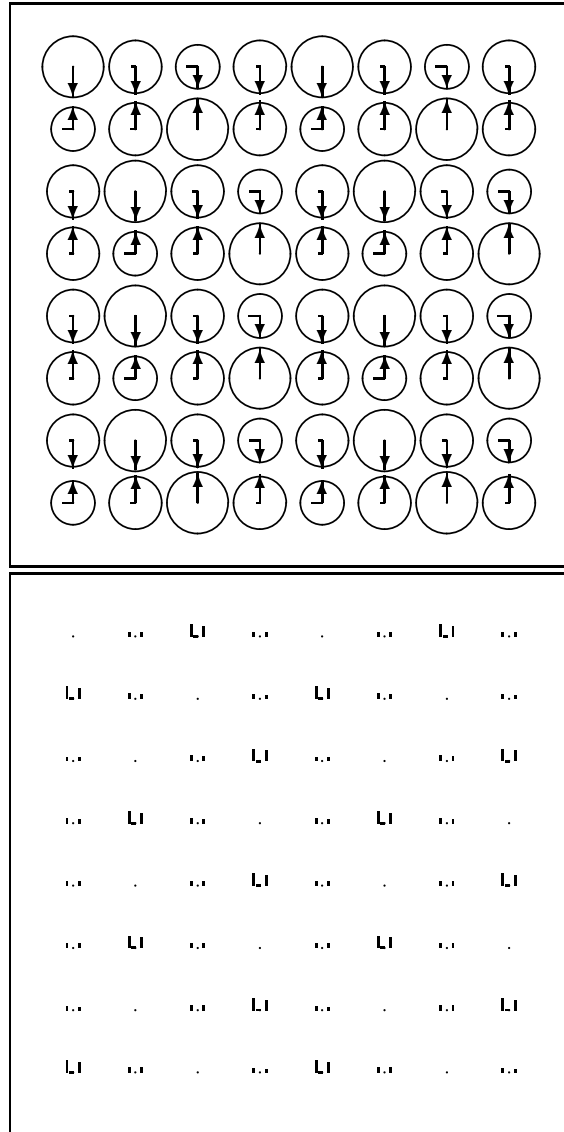


Figure 2. Weakly insulating C -AF phase (ferromagnetic horizontal lines coupled antiferromagnetically in vertical direction) as obtained for the doping $x = 1/4$ within the 8×8 cluster. Charge majority (undoped) sites have uniform charge distribution, with both x and z orbitals occupied and $S = 1$ spins; the charge minority sites are occupied by z electrons with spins $S = 1/2$ and show small JT distortions, Q_2 and Q_3 . Meaning of symbols and the values of parameters as in figure 1.

and slightly nonuniform orbital order (z orbital occupancy is then larger than x one on most sites in the cluster).

3.3. Large doping regime $1/3 < x \leq 1/2$

Coming to large doping regime $x > 1/3$, we have found further modifications of the C -AF spin order. First of all, the next doping level considered by us $x = 3/8$ is incompatible with the stripes shown in figure 3. As shown in figure 4, in this case the

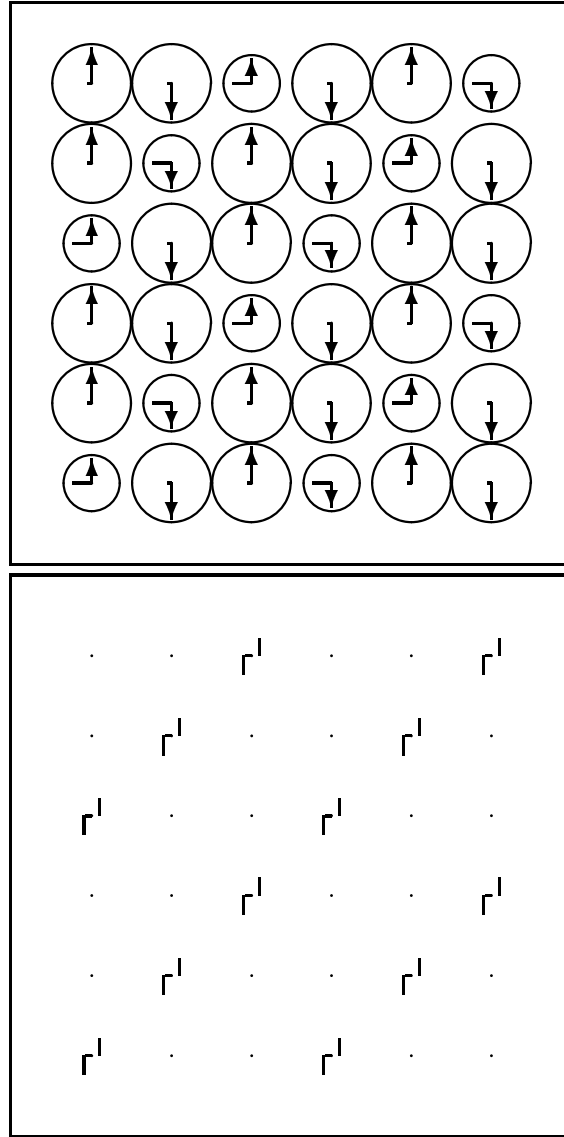


Figure 3. Insulating C -AF phase spin arrangement (ferromagnetic vertical lines coupled antiferromagnetically), with uniform charges on charge majority sites (spins $S = 1$ and both x and z orbitals occupied), as obtained for the $x = 1/3$ doping in 6×6 cluster. The charge minority sites form diagonal stripe boundaries. They are occupied by z electrons with spins $S = 1/2$ and they show small uniform Q_2 and Q_3 JT distortions. Meaning of symbols and the values of parameters as in figure 1.

ionic picture does not apply anymore and the electron charge is distributed uniformly. Therefore the values of the magnetic moments are close to $1.6 \mu_B$ per site, and the e_g orbitals are occupied in a similar way at all cluster sites. Hole doping reduces the electron density in x orbitals, therefore at the present doping level of $x = 3/8$ the ratio of electron density in x and z orbitals is close to 1:2. Unlike for lower doping level considered above, this electron distribution does not favor JT distortions at particular cluster sites with minority charge, and one finds uniform and rather small JT distortions at all the sites. Nevertheless, the electronic structure predicts that this ground state is

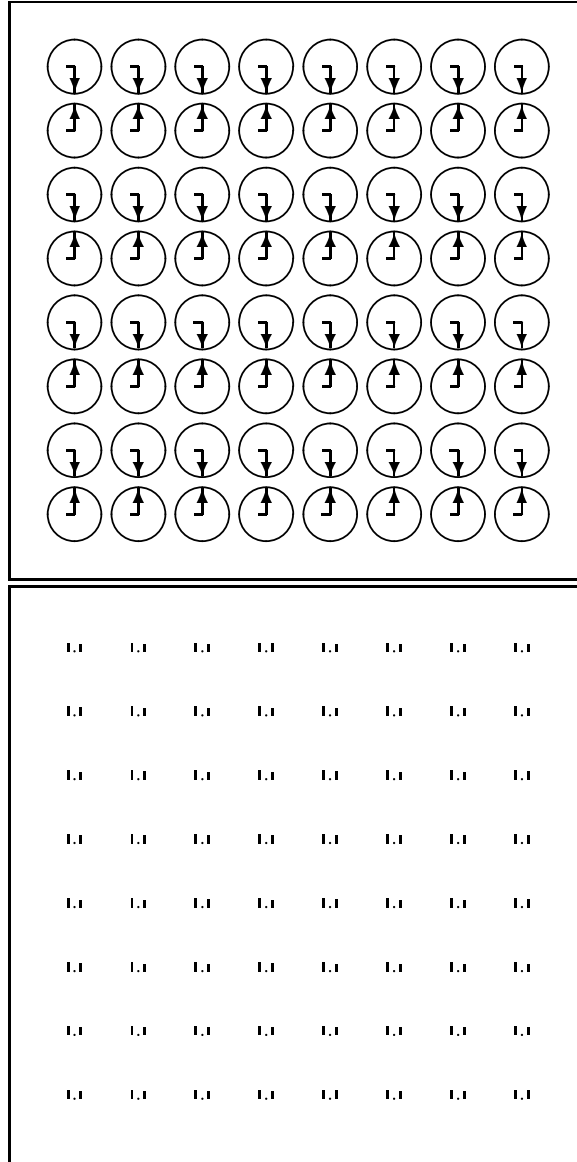


Figure 4. Almost perfect C -AF spin arrangement (like in figures 2-3) but with uniform charges, with about 1:2 x to z orbital order for e_g electrons and very small JT distortions, as obtained for $x = 3/8$ doping in 8×8 cluster. The pattern of JT distortions is almost uniform. Meaning of symbols and the values of parameters as in figure 1.

insulating, having a HOMO-LUMO gap $\Delta = 0.72$ eV.

The next physically interesting and experimentally much studied doping is half filling, i.e., $x = 1/2$. One finds that the C -AF spin order remains unchanged, but charge modulation develops. This doping level is compatible with a two sublattice structure in the charge ordered state shown in figure 5. The alternating electron charges are close to $n = 2$ and $n = 1$ on the majority and minority charge sites. Therefore, the ionic picture applies again to this doping level, and the system may be viewed as alternating charge order, with Ni^{2+} and Ni^{3+} ions on the two sublattices. This result reproduces

the experimental results [22, 23], with long-range checkerboard-like charge order found at half doping. Similar to all other cases, also this configuration is insulating, with a HOMO-LUMO gap $\Delta = 0.91$ eV.

The charge order found for $x = 1/2$ doping is closely followed by JT distortions, shown in figure 5. Large JT distortions at charge minority sites stabilize the checkerboard charge order in this case. Large $\{Q_{i2}\}$ distortions stabilize the charge order, and nonuniform electron distribution over e_g orbitals is stabilized by large $\{Q_{i3}\}$ distortions. As a result, x orbitals are almost empty at charge minority sites, and the occupancy of z orbitals is close to one electron at each site.

3.4. Maximal doping $x = 1$ for LaSrNiO_4

Experimental studies have established that for the examined class of $\text{La}_{2-x}\text{Sr}_x\text{NiO}_4$ compounds with large doping $x \simeq 1$, the ground state is paramagnetic and conducting [28], with a semiconductor-like conductivity (at low temperature close to zero Kelvin) [29]. We investigated this case using the present model by numerical computations, either using parameter set of table 1 or somewhat modified parameters. Extensive calculations have shown that reasonable values of parameters do not give results in agreement with experimental observations. In all considered cases one obtains perfect AF order, with homogeneous charge distribution (one electron per site) and with purely z -orbital occupation. In addition, the HOMO-LUMO gap is quite large $\Delta = 4.5$ eV (for the parameters from table 1).

While this theoretical result is very reasonable and may be expected taking the broken symmetry between two e_g orbitals in a monolayer LaSrNiO_4 system, it stimulates a question whether this result could invalidate all the previous results reported above. In our opinion the found disagreement of theory with experiment for such large doping level is only an indication that the effective model presented in this paper (without extra modifications) is too limited to perform satisfactorily. Our reasoning, based entirely upon experimental data, is twofold.

First of all, the conductivity at $x \simeq 1$ could be likely due to a completely other mechanism [29], namely to sample quality and near impossibility to grow perfect LaSrNiO_4 crystals. In reality what one grows are samples with oxygen vacancies (at vertices of NiO_6 octahedra). The level of oxygen vacancies is estimated to be at best 0.01 – 0.04 which seems enough to form a narrow donor band and therefore p -type conduction could set in. How this p -band destroys the AF order is another and difficult question. Still it is clear that the two-band model is not appropriate for the description of LaSrNiO_4 .

Second, the model computations are based on a formal scheme: the doping level is equal to fraction x in the actual chemical formula $\text{La}_{2-x}\text{Sr}_x\text{NiO}_4$. This is a common knowledge that possibly this is not true, similar as in $\text{YBa}_2\text{Cu}_3\text{O}_{6+x}$ superconductors [30], and most probably this simple-minded assumption works here reasonably well only for small values of x . (Note that the same fault can be attributed to modelling done

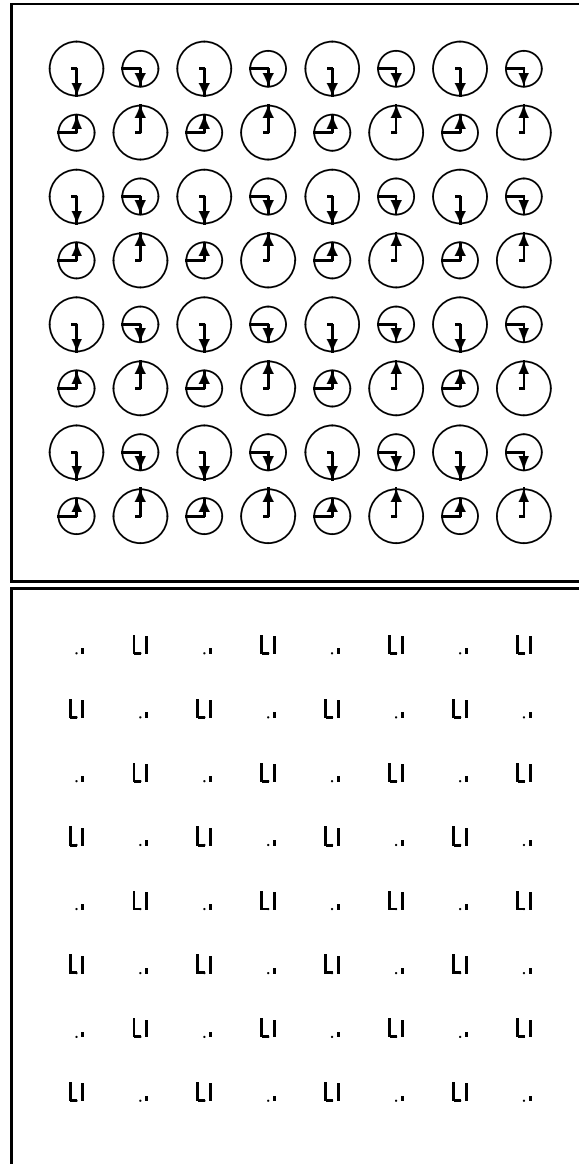


Figure 5. Perfect checkerboard crystal-like order with two sublattices, as obtained for $x = 1/2$ doping in 8×8 cluster. The C -AF spin order with alternating spin values between $S \simeq 1$ and $S \simeq 1/2$ spins for charge majority/minority sites, and holes doped into x orbitals at charge minority sites. Uniform electron distribution between x and z orbitals results in no JT distortions at charge majority sites, while considerable JT distortions at charge minority sites stabilize the orbital order with (almost) empty x orbitals. Meaning of symbols and the values of parameters as in figure 1.

in doped cuprates and manganites). Clearly, for larger doping one can expect sizable deviations between electron doping level and x fraction in chemical formula. These deviations depend on the type of the crystal lattice, the atom-atom distances, on the constituent atoms and no simple formula exists to compute them.

We suggest that the question whether the first or second explanation is more appropriate cannot be answered at present. It could be that both are partly valid

at the same time.

There are however some indications which can signal when and where the above proportionality between doping level and the chemical concentration x could not be obeyed. In our particular case such indications can be read out from ref. [31] where the true quantum-chemistry *ab-initio* computations (HF, BLYP and PBE) for LaNiO_3 were performed (using CRYSTAL06 computer code) and where Mullikan population analysis was done. This is a different (three-dimensional) conducting substance, not the one studied in this paper, but still the problem is more or less the same. The Mullikan charges found on Ni atoms are $\simeq +1.7$ instead of formal +3 and on oxygens the Mullikan charges are $\simeq -1.2$ instead of formal -2. It is true that Mullikan charges are only a rather crude estimate but still from the above *ab-initio* data it follows that the effective model with formal occupied with one d -electron-type Wannier function (per site) is not correct for LaNiO_3 .

One can envisage the modification of our model which possibly could work properly for the description of LaSrNiO_4 . It seems necessary to supplement the model with at least one extra Wannier orbital per site. For the first trial, in the spirit of the Anderson lattice model, this could be a simple s -type Wannier orbital of the oxygen type (assuming spherically symmetric distribution of the oxygen p electrons around the central nickel). The new extra Hamiltonian terms would be simple kinetic s -type nearest-neighbour hopping supplemented by $s - d$ hybridization. According to the Koster-Slater rules, the $s - d$ hybridization on single lattice site vanishes and one should consider it between nearest-neighbour sites only. This goes however beyond the scope of the present paper and is planned as a separate future investigation.

4. Crucial role played by Jahn-Teller distortions

4.1. Finite Jahn-Teller coupling g_{JT}

We already remarked several times on the importance of JT coupling. Here we try to draw some more general conclusions and provide extra information.

Test computations for the undoped La_2NiO_4 substance ($x = 0$) invariably (independently of the initial conditions) give insulating G -AF ground state (for $S = 1$ spins) with uniform charge distribution and equal occupation of x and z orbitals, in perfect agreement with experiment [32, 33]. In this state no JT distortions can arise. This result was obtained for almost any set of the Hamiltonian parameters with one notable exception. For too large JT coupling, in particular for $g_{\text{JT}} > 3.5 \text{ eV } \text{\AA}^{-1}$ (while the other Hamiltonian parameters are those from the table 1) nonmagnetic phase starts to develop. The emerging nonmagnetic sites feature equal occupation of 0.5 electron per up and down spin both for x and z orbitals. This is accompanied by huge and clearly unphysical JT distortions of the Q_2 type. For $g_{\text{JT}} = 3.8 \text{ eV } \text{\AA}^{-1}$ the common magnetic sites with spin $S = 1$ (and zero JT distortions) are already quite scarce and the nonmagnetic sites do abound. We suggest that for so large values of g_{JT} the simplified

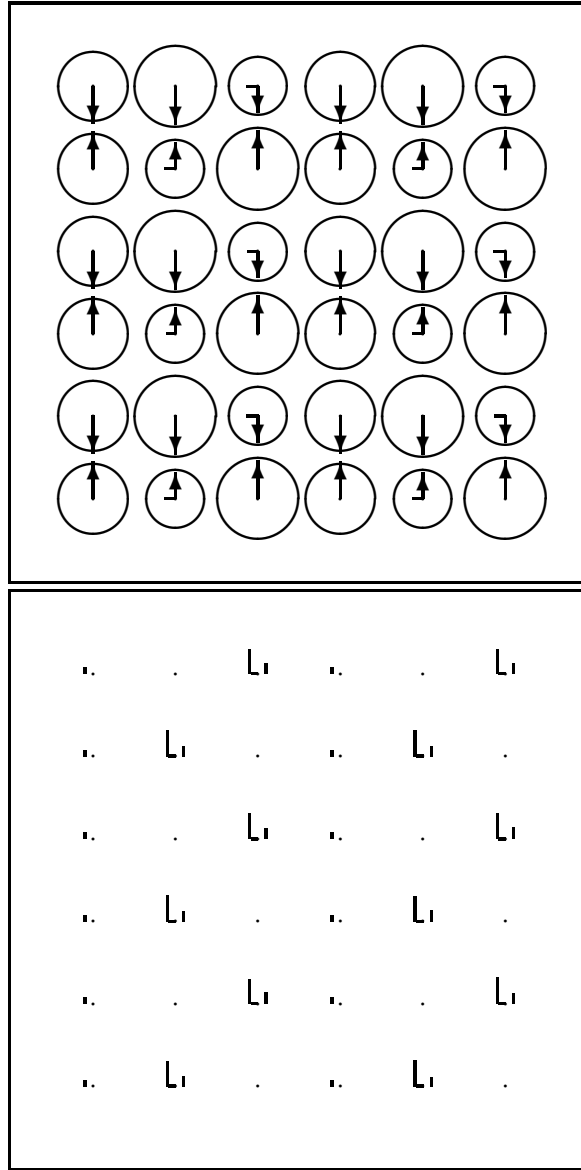


Figure 6. Insulating ground state obtained for the 6×6 cluster with $x = 1/3$ doping and zero crystal field ($E_z = 0$). The C -AF order develops, with spins $S = 1$ and uniform charge distribution (the same electron density in x to z orbitals) on undoped sites and lower spins on charge minority sites. The charge minority sites do not form here diagonal stripe boundaries (as in figure 3) but the superlattice with long-range order develops what is better visible on the lower panel. Meaning of symbols and the values of other parameters as in figure 1.

form of JT Hamiltonian which we use is not proper for correct description of JT effects i.e., eq. (4), and in particular the simple form of the coupling to the lattice in eq. (4) requires substantial corrections.

Further, extensive tests for $x = 1/3$ doped substance revealed that only in a narrow region of $2.8 < g_{\text{JT}} < 3.2$ (in $\text{eV}\text{\AA}^{-1}$ units) diagonal stripes do form. Hence, the role of the JT distortions is crucial for stripe formation. Furthermore, it was also interesting to

establish that for zero crystal field, $E_z = 0$, the diagonal stripes disappear, though the charge, orbital and magnetic order remains almost the same like the one for the standard parameters listed in table 1 (see figure 6, compare with figure 3). The resulting phase is insulating, with the HOMO-LUMO gap $\Delta = 0.58$ eV. (This is a somewhat similar scenario like the one reported in $Nd_{1.67}Sr_{0.33}NiO_4$ [34]).

However, when one switches to smaller values of the on-site Coulomb repulsion, for example taking $U = 5$ eV and $E_z = 0$, diagonal stripes reappear again (i.e., when all the other parameters $\{t, J_H, g_{JT}, K\}$ have the values given in table 1). The value $U = 5$ eV corresponds to suggestion that screening of U by hybridization with oxygen orbitals is larger than usually assumed. It follows that the diagonal stripes do not appear for any set (or even in a broad range) of the Hamiltonian parameters, but result from a subtle balance between several competing mechanisms. Furthermore, it is difficult to conclude what is more proper for our nickelate model, either $U/t \approx 8$ or rather a higher value $U/t \approx 12$ ($U/t \approx 12$ was our preference for the bulk of the computations).

4.2. Setting Jahn-Teller coupling to zero $g_{JT} = 0$.

For zero JT coupling $g_{JT} = 0$ and small doping $x = 1/8$ we detected no change in the ground state — it looks just like the one shown in figure 1 (resulting from the computations performed for the standard parameter set of table 1) and is insulating.

The situation changes somewhat for higher doping. While for two doping levels, $x = 1/4$ and $x = 3/8$, the ground states remain very similar to the ones obtained before, i.e., the C -AF order is accompanied by small charge modulation, when the JT distortions are absent the $x = 1/4$ state is metallic, opposite for the state for doping $x = 3/8$, where a relatively large gap $\Delta \simeq 0.7$ eV separates the HOMO and LUMO states in the 8×8 cluster. For other larger dopings (up to $x = 1/2$) the ground states are conducting.

This result, i.e., the exception obtained for $x = 3/8$, is puzzling and could be either a finite size effect and/or an indication of quite different electron correlation energies in systems with different electron number. Here it seems that a full explanation and a few digressions are proper. To be precise we performed control computations in 8×8 cluster doped with 26 holes (quite close to 24 holes which correspond to $x = 3/8$). The true ground state was conducting. Then we performed another set of control computations in 6×6 cluster doped with 14 holes. (This is as close as possible to $3/8$ doping in 8×8 cluster). This time the situation was a little bit more complicated. The best HF ground state (charge homogeneous with well developed C -AF order) was found to be insulating. The corresponding correlation energy correction was rather small. However, for a group of higher HF energy levels (with a similar but non-perfect ordering and with HOMO-LUMO gap being about 0.1 eV, i.e., possibly conducting) much stronger correlations develop and when included the total energy turned out to be lower than that obtained for the first HF ground state plus its correlation energy. In other words for 6×6 and for doping $x \approx \frac{3}{8}$ the true ground state is conducting and strong correlations

are responsible for that. Why the same situation was not found for 8×8 cluster can, possibly, be due to poor selection of the local operators (within local ansatz), see eq. 12 which could be thus responsible for not catching some sizable part of total correlation energy. In other words mean-field type treatment of correlations (which we employ) could be not enough, and the true physical picture is that various contributions to correlation energy are highly non-homogeneous and strong in the doped, charge and spin non-homogeneous, nickelates.

As the closing remarks to this lengthy digression let us mention that similar control computations were performed in 6×6 clusters for different dopings — the results corroborated the results obtained in 8×8 clusters (the $x = \frac{3}{8}$ doping was the only exception).

Now, let us return back to the main subject and other doping levels. For $x = 1/2$ the ground state is again an experimental checkerboard: one finds a two-sublattice arrangement, exactly like the one displayed in the top panel of figure 5. The long range charge and orbital order are both close to being perfect here. This demonstrates that the checkerboard phase can form by a purely electronic mechanism, and the JT distortions only make this state more robust. (For zero JT coupling this state is also conducting).

As mentioned before, for doping $x = 1/3$, one obtains a conducting ground state with $g_{\text{JT}} = 0$, i.e., the HOMO-LUMO gap is $\Delta = 0.03$ eV. The obtained phase shows a slightly non-homogeneous C -AF order which looks very similar to the upper panel on figure 2. The true long-range order is however not present and diagonal stripes do not appear.

5. Summary and conclusions

Let us address the correlated wave functions first. As expected the correlation effects turned out to be much stronger here than in the manganites [24]. This could be recognized by investigating nonmagnetic states, where the energy is dramatically reduced by the correlation effects (not shown). In the states with either G -AF (for $x = 0$) or C -AF order (for $0 < x \leq 0.5$) the correlation energy is rather small as the magnetic states are well developed. This demonstrates that the Hartree-Fock approximation provides a realistic energy estimate for the states with broken symmetry when the Coulomb interactions are strong. A similar situation was also found in the two-band model for superconducting cuprates [35].

Coming to detailed analysis, the obtained energies of the ground state found in the Hartree-Fock approximation and using the local ansatz are shown in table 2. In each case the correlation energy, $E_{\text{corr}} = E_{\text{HF}} - E_{\text{tot}}$ is rather small. The insulating gap exhibits a non-monotonous behavior: it is large for the undoped La_2NiO_4 compound ($x = 0$), with a HOMO-LUMO gap of 7.42 eV (see table 2). It drops to 1.86 eV for $x = 0.125$, and becomes rather small for $x = 0.25$, where we found a local minimum of 0.28 eV. In case of the stripe phase at $x = 1/3$ it is again larger (note that the size of the cluster 6×6 is different here, but this should not influence significantly the estimated

Table 2. Energies obtained for the insulating ground states in the Hartree-Fock approximation, E_{HF} , and for correlated wave functions, E_{tot} , as well as the HOMO-LUMO gap Δ obtained for representative doping levels (all in eV). Last row shows the prediction of the model for LaSrNiO_4 ($x = 1$) — this result does not correlate well with experiment, see section 3.4.

x	cluster	E_{HF}	E_{tot}	Δ
0.000	8×8	263.64	263.54	7.42
0.125	8×8	221.87	221.63	1.86
0.250	8×8	179.95	178.90	0.28
0.333	6×6	85.14	84.31	0.57
0.375	8×8	136.08	134.96	0.72
0.500	8×8	95.14	93.29	0.91
1.000	8×8	-46.17	-46.18	4.52

gap Δ), and next increases steadily up to $\Delta = 0.91$ eV at $x = 0.5$. This confirms the experimental observation that $\text{La}_{2-x}\text{Sr}_x\text{NiO}_4$ nickelates are insulators [32] in the entire doping regime up to half-doping $x = 1/2$.

The role of JT distortions for the phase situation in $\text{La}_{2-x}\text{Sr}_x\text{NiO}_4$ was discussed in the literature [12, 19], but the results are controversial to some extent. In ref. [19] the stripes were attributed to Jahn-Teller distortions but in ref. [12] it was argued (for the model explicitly featuring oxygens in-between nickel atoms) that Jahn-Teller distortions are not consistent with the local symmetry and with the experimental results. Our simple effective model is not able to resolve this controversy and to answer the question concerning the origin of the stripe phase found at $x = 1/3$ doping as it considers distortions as being independent from one another (i.e., not cooperative). Still within the framework of the present model we support the claim by Hotta and Dagotto [19] that Jahn-Teller distortions are essential for the development of the stripe order for the doping $x = 1/3$. On the other hand, other results of our computations show that the short range order (on average) does not change due to the lattice distortions, and it is only the global population of $3z^2 - r^2$ orbitals at defect sites and long range order which are stabilized by the Jahn-Teller effect.

The results of the present study uncover the fundamental difference between the stripes in cuprates and in nickelates. While a competition between the magnetic energy (superexchange) and the kinetic energy of doped holes drives the stripe structures in doped cuprates [3] with site-centered structures [36, 37], or could also be responsible for stripes in certain t_{2g} systems [13], this mechanism is absent in layered nickelates for two reasons: (i) when hole doping occurs in d^8 (instead of d^9) configuration, the ions occupied by holes carry a spin 1/2 of the remaining e_g electron and participate in the magnetic order, and (ii) the doped ions are active for the Jahn-Teller effect and local distortions form around them. Both these effects suppress the kinetic energy of the doped holes and the competition between the magnetic and kinetic energy is absent.

Therefore, the stripes cannot form at low doping (up to $x = 0.25$ considered here) but this regime is dominated by isolated charge defects stabilized by local lattice distortions. The doping $x = 1/3$ is the first one where the doped sites have to appear as next nearest neighbours, and they order in form of a stripe phase. We suggest that the electronic structure has a local minimum for this phase rather than for a random distribution of doped sites. This pattern does not hold at higher doping $x = 0.375$, but decides about the stability of the checkerboard phase at the doping $x = 0.5$, where again the configurations with doped ions being next nearest neighbours to one another occur along both diagonal directions. Altogether, the diagonal stripe pattern for $x = 1/3$ is thus favoured by the characteristic properties of doped holes in layered nickelates which avoid each other.

Summarizing, the main virtue (in our opinion) of this paper is a demonstration that the same model which worked very well for doped perovskite manganites [24] performs equally well for the layered nickelates. It helped to identify the leading mechanism, being the Jahn-Teller effect in presence of strong local correlations, responsible for the stripe phase which occurs only at the $x = 1/3$ doping and for the checkerboard phase found at the $x = 1/2$ doping. At the same time some open questions still remain which could be resolved by future studies. In particular, it would be interesting to perform a theoretical study with cooperative Jahn-Teller distortions including explicitly oxygen ions. Furthermore, it would be very helpful in future theoretical modeling of doped nickelates if a more precise relation between the electron doping level (used in computations) and the chemical doping (such as follows from the chemical formula) could be established.

Acknowledgments

We acknowledge financial support by the Polish Ministry of Science and Higher Education under Project No. N202 104138. A M Oleś was also supported by the Foundation for Polish Science (FNP).

References

- [1] Zaanen J and Gunnarsson O 1989 *Phys. Rev. B* **40** 7391
Poilblanc D and Rice T M 1989 *Phys. Rev. B* **39** 9749
Kato M, Machida K, Nakanishi H and Fujita M 1990 *J. Phys. Soc. Jpn.* **59** 1047
Zaanen J and Oleś A M 1996 *Annalen der Physik* **5** 224
- [2] Tranquada J M, Sternlib B J, Axe J D, Nakamura Y and Uchida S 1995 *Nature (London)* **375** 561
- [3] Kivelson S A, Bindloss I P, Fradkin E, Oganessian V, Tranquada J E, Kapitulnik A and Howald C 2003 *Rev. Mod. Phys.* **75** 1201
Raczowski M, Frésard R and Oleś A M 2006 *Low Temp. Phys.* **32**, 305
Vojta M 2009 *Adv. Phys.* **58** 699
- [4] Oleś A M 2010 *Acta Phys. Polon. A* **118** 212
- [5] Góra D, Rościszewski K and Oleś A M 1999 *Phys. Rev. B* **60** 7429
Rościszewski K and Oleś A M 2003 *J. Phys.: Condensed Matter* **15** 8363

- [6] Fleck M, Lichtenstein A I, Pavarini E and Oleś A M 2000 *Phys. Rev. Lett.* **84** 4962
Fleck M, Lichtenstein A I and Oleś A M 2001 *Phys. Rev. B* **64** 134528
- [7] Raczkowski M, Frésard R and Oleś A M 2006 *Phys. Rev. B* **73**, 174525
Raczkowski M, Frésard R and Oleś A M 2006 *Europhys. Lett.* **76** 128
- [8] Dagotto E, Hotta T and Moreo A 2001 *Physics Reports* **344** 1
Dagotto E 2005 *New J. Phys.* **7** 67
- [9] Weisse A and Fehske H 2004 *New J. Phys.* **6** 158
- [10] Tokura Y 2006 *Rep. Prog. Phys.* **69** 797
- [11] Hotta T, Feiguin A and Dagotto E 2001 *Phys. Rev. Lett.* **86** 4922
- [12] Hotta T and Dagotto E 2004 *Phys. Rev. Lett.* **92** 227201
- [13] Wróbel P and Oleś A M 2010 *Phys. Rev. Lett.* **104** 206401
- [14] Krüger F, Kumar S, Zaanen J and van den Brink J 2009 *Phys. Rev. B* **79** 054504
- [15] Tranquada J M, Buttrey D J, Sachan V and Lorenzo J E 1994 *Phys. Rev. Lett.* **73** 1003
Sachan V, Buttrey D J, Tranquada J M, Lorenzo J E and Shirane G 1995 *Phys. Rev. B* **51** R12742
- [16] McQueeney R J, Bishop A R, Yi Ya-Sha and Yu Z G 2000 *J. Phys.: Condensed Matter* **12** L317
- [17] Zaanen J and Littlewood P B 1994 *Phys. Rev. B* **50** 7222
- [18] Raczkowski M, Frésard R and Oleś A M 2006 *Phys. Rev. B* **73** 094429
- [19] Yamamoto S, Fuiwara T and Hatsugai Y 2007 *Phys. Rev. B* **76** 165114
- [20] Mazin I I, Khomskii D I, Lengsdorf R, Alonso J A, Marshall W G, Ibberson R M, Podlesnyak A, Martinez-Lope M J and Abd-Elmeguid M M 2007 *Phys. Rev. Lett.* **98** 176406
- [21] Schwingenschlögl U, Schuster C and Frésard R 2008 *Europhys. Lett.* **81** 27002
Schwingenschlögl U, Schuster C and Frésard R 2009 *Europhys. Lett.* **88** 67008
- [22] Chen C H, Cheong S-W and Cooper A S 1993 *Phys. Rev. Lett.* **71** 2461
Tranquada J M, Buttrey D J and Sachan V 1996 *Phys. Rev. B* **54** 12318
Kajimoto R, Kakeshita T, Yoshizawa H, Tanabe T, Katsufuji T and Tokura Y 2002 *Appl. Phys. A* **74** (suppl.) S1765
Yoshizawa H, Kakeshita T, Kajimoto R, Tanabe T, Katsufuji T and Tokura Y 2000 *Phys. Rev. B* **61** R854 (2000)
Freeman P G, Boothroyd A T, Prabhakaran D, Gonzalez D and Enderle M 2002 *Phys. Rev. B* **66** 212405
Kaimoto R, Ishizaka K, Yoshizawa H and Tokura Y 2003 *Phys. Rev. B* **67** 014511
- [23] Vigliante A, von Zimmermann M, Schneider J R, Frello T, Andersen N H, Madsen J, Buttrey D J, Gibbs D and Tranquada J M 1997 *Phys. Rev. B* **56** 8248
Du C H, Hhazi M E, Su Y, Hatton P D, Brown S D, Stirling W G, Cooper M J and Cheong S-W 2000 *Phys. Rev. Lett.* **84** 3911
Hatton P D, Ghazi M E, Wilkins S B, Spencer P D, Mannix D, d'Almeida T, Prabhakaran P, Boothroyd A T and Cheong S-W 2002 *Physica B* **318** 289
Ghazi M E, Spencer P D, Wilkins S B, Hatton P D, Mannix D, Prabhakaran D, Boothroyd A T and Cheong S-W 2004 *Phys. Rev. B* **70** 144507
Spencer P D, Ghazi M E, Wilkins S B, Hatton P D, Brown S D, Prabhakaran D and Boothroyd A T 2005 *Eur. Phys. J. B* **46** 27
- [24] Rościszewski K and Oleś A M 2007 *J. Phys.: Condensed Matter* **19** 186223
Rościszewski K and Oleś A M 2008 *J. Phys.: Condensed Matter* **20** 365212
Rościszewski K and Oleś A M 2010 *J. Phys.: Condensed Matter* **22** 425601
- [25] Oleś A M 1983 *Phys. Rev. B* **28** 327
- [26] Popovic Z and Satpathy S 2000 *Phys. Rev. Lett.* **84** 1603
- [27] Stollhoff G and Fulde P 1980 *J. Chem. Phys.* **73** 4548
Stollhoff G 1996 *J. Chem. Phys.* **105** 227
Fulde P 1991 *Electron Correlations in Molecules and Solids*, Springer Series in Solid State Sciences, Vol. **100** Springer Verlag, Berlin.

- [28] Cava R J, Batlogg B, Palstra T T, Krajewski J J, Peck Jr. W F, Ramirez A P and Rupp Jr. L W 1991 *Phys. Rev. B* **43** 1229
- [29] Ivanova T A, Jacyna-Onyszkiewicz I and Yablokov Yu V 2002 *Physics of the Solid State* **44** 1622
- [30] Zaanen J, Paxton A T, Jepsen O and Andersen O K 1988 *Phys. Rev. B* **60** 2685
- [31] Masys S, Mickievicius S, Greboinskij S and Jonauskas V 2010 *Phys. Rev. B* **82** 165120
- [32] Thanh T D and Hong L V 2008 *J. Korean Phys. Soc.* **52** 1456
- [33] Buttrey D J, Honig J M and Rao C N R 1986 *J. Solid State Chem.* **64** 287
- [34] Hücker M, Gu G D, Tranquada J M, v. Zimmermann M, Klauss H -H, Curro N J, Braden M and Büchner B 2007 *Physica C* **460-462** 170
- [35] Oleś A M and Zaanen J 1988 *Phys. Rev. B* **39** 9175
- [36] Tranquada T M, Gu G D, Hücker M, Jie Q, Kang H-J, Klingeler R, Li Q, Tristan N, Wen J S, Xu G Y, Xu Z J, Zhou J and v. Zimmermann M 2008 *Phys. Rev. B* **78** 174529
- [37] Greiter M and Schmidt H 2010 *Phys. Rev. B* **82** 144512